Research Paper
International Journal of Aerospace System Engineering
Vol.5, No.2, pp.8-15 (2018)

ISSN 2383-4986
EISSN 2508-7169
https://doi.org/10.20910/IJASE.2018.5.2.8

A 3-axis Focus Mechanism of Small Satellite Camera Using Friction-Inertia Piezoelectric Actuators

Dae Gi Hong, Jai Hyuk Hwang†
Dept. of Mechanical and Aerospace Engineering, Korea Aerospace University, Korea
KOREA, SEOUL
†*E-mail:jhhwang@kau.ac.kr*

Abstract

For small earth observation satellites, alignment between the optical components is important for precise observation. However, satellite cameras are structurally subject to misalignment in the launch environment where vibration excitations and impacts apply, and in space environments where zero gravity, vacuum, radiant heat and degassing occur. All of these variables can cause misalignment among the optical components. The misalignment among optical components results in degradation of image quality, and a re-alignment process is needed to compensate for the misalignment. This process of re-alignment between optical components is referred to as a refocusing process. In this paper, we proposed a 3 - axis focusing mechanism to perform the refocusing process. This mechanism is attached to the back of the secondary mirror and consists of three piezoelectric inertia-friction actuators to compensate the x-axis, y-axis tilt, and de-space through three-axis motion. The fabricated focus mechanism demonstrated excellent servo performance by experimenting with PD servo control.

Key Words : Small Satellite Camera, Misalignment, Re-focusing, Focus Mechanism, Piezoelectric Inertia-Friction Actuator (PIFA)

1. Introduction

The early Earth observation satellites required high resolution images for military purposes, and correspondingly the size of the developed optical cameras to be very large. However, such large satellites required tremendous costs for production and testing. Considering that the life span of low orbit observation satellites is about 5 years, development and operation maintenance cost of large satellites is inefficient compared to small satellites. These large satellites were faced with efficiency problems as their performance versus operational and development costs became expensive. As a result, during the 1990s in the United States, the research of small, high resolution satellites began [1]. This trend has continued, and today we say miniaturized spacecrafts as well. Thanks to the development of electronic and mechanical industries, the performance of components has improved, and prices have been lowered. Together, these reasons provide an environment suitable for miniaturization of satellites [2].

However, as satellites are miniaturized, there is a disadvantage that small satellites are structurally weaker than medium and large sized ones. In launch and space environments, satellites are affected by vibration, impact, extreme thermal changes, and de-gassing of structures in a vacuum state. These influences cause relative distances between the optical components and degrade the image quality they provide [3]. Especially, in a Cassegrain type optical system, the relative distance between the primary mirror and the secondary mirror must be kept within a submicron. However, in the case of small satellites, it is difficult to maintain the initial

Received: Aug. 20, 2018 Revised: Oct. 03, 2018 Accepted: Oct. 04, 2018
† Corresponding Author
Tel: +82-2-300-0109, E-mail: jhhwang@kau.ac.kr

alignment state because of the limitation of the stiffness of the structure. Therefore, there is a need for a refocusing process that realigns the relative distance between the optical components on the on-orbit. The relative distance between optical components when alignment is disturbed by deformation of the optical structure is called misalignments. There are three types of misalignments: tilt, center, and space. With respect to the primary mirror, de-space means a misalignment in the optical axis direction, and the tilt means that an angle is generated between the optical components. De-center means that the center of the optical component deviates from the optical axis with respect to the vertical plane of the optical axis.

In the satellite optical system, a mechanism for re-focusing is called a focus mechanism, and it is classified into a servo drive type mechanism and a thermal control type mechanism. The servo-driven mechanism mainly performs re-focusing using step motors and piezoelectric actuators. The SPOT series developed by CNES and SEVIRI, the optical payload of MSG satellite developed by ESA, and the Spitzer Space Telescope developed by NASA, are satellites to which the servo driven mechanism is applied[4]. The thermal control mechanism uses a heater to generate thermal deformation of the optical structure to perform refocusing [5]. The satellites to which the thermal control mechanism is applied are the Pleiades series developed by CNES and the KOMPSAT series satellite developed in Korea. The thermal control focus mechanism is simple in structure and low in risk, but it has weakness such as a long operating time and continuous power consumption. The servo-driven focus mechanism is free from the configuration of the actuators and the controller, has a short time for operation and can secure a wide driving range. On the other hand, it is difficult to implement a servo-driven mechanism that has proven stability and reliability in launch and space environment.

The focus mechanism proposed in this study can perform 3-axis motion for de-space and tilt by using three piezoelectric inertia-friction actuators (PIFAs), which enables precise refocusing compared to other focus mechanisms. The target optical system to which the focus mechanism is applied is selected as a Schmidt-Cassegrain type optical system. To efficiently utilize the space of the Cassegrain type optical system, a focus mechanism is installed by using a shielded space behind the secondary mirror.

In this study, we designed and fabricated a 3-axis focus mechanism for a small satellite camera using friction-inertia piezoelectric actuators. First, we set up requirements for focus mechanism according to the misalignments caused by the sources of vibration of the satellites [6]. A flexure was installed between the mechanism part and the Schmidt plate to prevent damage to the optical components caused by the impact of the launch process and the thermal environment in the space. It was designed in consideration of the precise mechanism motion and the minimum wave front error on the mirror surface using a kinematic analysis of the mechanism and the opto-mechanical analysis. The mathematical model was obtained by analyzing the structure of the PIFA used in the focus mechanism and confirmed by comparing with the experimental model obtained through the open loop experiment. We also designed a PD controller to improve the transient response and steady-state error of the focus mechanism. For the servo performance verification of this mechanism, a mock-up for the focus mechanism was made and a servo performance experiment of the focus mechanism was performed through LabView.

2. Focus Mechanism Design

2.1. Target Optical System Design

The optical system of Earth observation satellites is limited in weight and size, so Cassegrain type optical systems will mainly be used. Earth observing satellites are also prone to misalignment of optical structures due to harsh launch and space environments. To compensate for misalignment errors, micrometer alignment errors are allowed from the initial alignment state of the satellite camera, and a focus mechanism is installed using a shielded space behind the secondary mirror [7, 8]. The Cassegrain optical system is advantageous for miniaturization because the length of the optical system is short. The Schmidt-Cassegrain optical system which is a Cassegrain type application has a Schmidt plate attached to the front of the lens tube to improve optical performance by correcting various aberrations. However, the Schmidt-Cassegrain optical system requires a field flattener lens group for correcting distortion at the edge of the focal plane.

The design process of the optical system proceeds in the order of selection of major requirements, optical system design, and performance analysis. First, we set the size of the primary mirror to satisfy the requirements, and then designed the optical components considering the specifications of the optical parts such as the detector and secondary mirror. In this study, the target optical system was adopted as a small satellite equipped with an optical system with a primary mirror diameter of 200 mm. Observation altitude was set at 685 km above sea level, taking into consideration the altitude of most earth observation satellites [9]. The target

performance of the optical system is set to a swath width of 12 km, GSD of 2.8 m, F # of 10, EFL of 2,000 mm, and observation bandwidth of 450 to 650 nm, which is a visible light band. Detectors used in satellite cameras are classified into scanning type, push-broom type, framing type, and imaging spectrometer type depending on the arrangement of sensors. Fig. 1 shows the shape according to the type of detector [10]. In this study, we used the CMOS sensor of Cannon's EOS-5D camera, a commercial DSLR, for cost reduction and ease of fabrication.

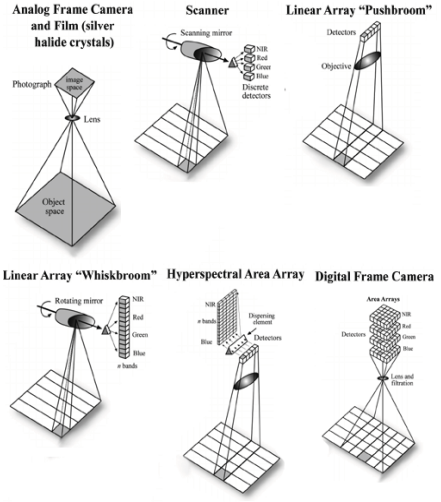

Fig. 1 Sensor Types of Earth Observation Camera

The design of the target optical system is based on the requirements, and the optical design program Code V is used for the design. The MTF performance of the entire optical system is designed to satisfy requirements of 10% or more. Therefore, the MTF performance of the electronic system such as the detector is assumed to be 40%, and the MTF performance of the target optical system is designed to satisfy 30% or more. In addition, the spot diagram and the field curve were confirmed as performance indicators.

2.2. Kinematic Design of Focus Mechanism

The proposed focus mechanism consists of three PIFAs and three LVDTs. Fig. 2 is the CAD shape of the focus mechanism using PIFA.

Fig. 2 Focus Mechanism Using PIFA

The working principle of the focus mechanism is that if three PIFAs generate the same amount of displacement, only de-space occurs, and if they generate different amounts of displacement in each PIFA, tilt occurs. In this study, the kinematic relationship between the motion (de-space and x, y-axis tilt) of the secondary mirror and PIFA and LVDT can be defined using the following plane equation.

$$ax_i + by_i + cz_i + d = 0,\ (\mathrm{i} = 1,\ 2,\ 3) \tag{1}$$

$$\text{Despace} = \frac{z_1 + z_2 + z_3}{3} \tag{2}$$

In the above equation (1), z_1, z_2 and z_3 are the displacement values of the respective LVDTs. (x_1, y_1), (x_2, y_2) and (x_3, y_3) is the position of each LVDT arranged in the focus mechanism. Equation (2) is the definition of the generated de-space. The coefficients a, b, and c used in equation (1) are expressed as follows.

$$\mathrm{a} = \frac{1 + y_1 b + z_1 c}{x_1} \tag{3}$$

$$\mathrm{b} = \frac{x_3 - x_1 - (x_1 z_3 - x_3 z_1)c}{x_3 y_1 - x_1 y_3} \tag{4}$$

$$\mathrm{c} = \frac{x_1(y_2 - y_3) - x_2(y_1 - y_3) + x_3(y_1 - y_2)}{x_1(y_2 z_3 - y_3 z_2) - x_2(y_1 z_3 - y_3 z_1) + x_3(y_1 z_2 - y_2 z_1)} \tag{5}$$

(a, b, c) shown in the above equations (3)-(5) is normal vector perpendicular to the plane, and the constant term d is canceled out because it is a common term for equations (3)-(5). Normal vector and de-space can be calculated by substituting the position values of LVDT. The θ_x and θ_y can be obtained as follows by inner products of the derived normal vector and the basis vectors of the x and y-axis.

$$\theta_x = cos^{-1}\left(\frac{\vec{n}\cdot\overrightarrow{b_x}}{|\vec{n}||\overrightarrow{b_x}|}\right) \quad (6)$$

$$\theta_y = cos^{-1}\left(\frac{\vec{n}\cdot\overrightarrow{b_y}}{|\vec{n}||\overrightarrow{b_y}|}\right) \quad (7)$$

In equations (6) and (7), $\vec{n}$ is the normalized normal vector obtained from equations (3)-(5), and $\overrightarrow{b_x}$ and $\overrightarrow{b_y}$ are the basis vectors of each axis. Using equations (2), (6) and (7), the x and y-axis tilt, and de-space values of the secondary mirror can be calculated for the displacement of each LVDT during the focus mechanism operation. Similarly, we can calculate the displacements of the PIFAs by inversely calculating the relation between the displacement values of the LVDTs and those of the PIFAs. In this study, the proposed focus mechanism consists of three PIFAs arranged at equal intervals of 120° along the circumference with a radius of 20 mm on the base plate (installation plane), and the LVDTs are installed at a difference of 60° from each of the corresponding PIFAs. Fig. 3 shows the computation process of the tilt and de-space when the displacements of PIFAs are given. Table 1 shows the displacements of PIFAs required when only tilt is considered.

Table 1 Actuator Displacements Required for Assigned Tilts

Tilt (μrad)		#1 (μm)		#2 (μm)		#3 (μm)	
x	y	LVDT	PIFA	LVDT	PIFA	LVDT	PIFA
0	100	-1	-2	-1	1	2	1
0	200	-2	-4	-2	2	4	2
100	0	1.73	0	-1.73	1.73	0	-1.73
200	0	3.46	0	-3.46	3.46	0	-3.46
100	100	0.73	-2	-2.73	2.73	2	-0.73
200	200	1.46	-4	-5.46	5.46	4	-1.46

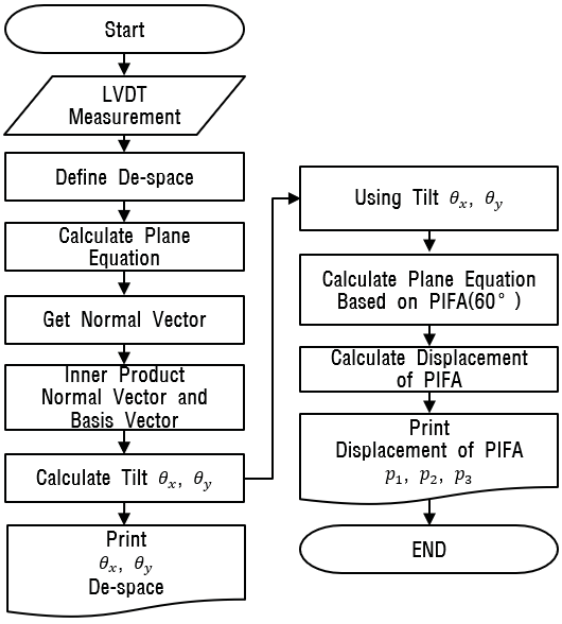

Fig. 3 Flowchart for Tilt and De-space Calculation

2.3. Opto-Mechanical Design of Focus Mechanism

The deformation of the optical structure in launch and space environment as well as the displacements of the actuators of the focus mechanism affect the secondary mirror surface. This influence is greater than the machining accuracy of the optical component surface, and thus introduces minor deformation of the secondary mirror surface. Therefore, it is necessary to attach a flexure between the secondary mirror and the PIFAs to minimize mechanical deformation, thereby preventing image distortion.

The opto-mechanical design process consists of a finite element analysis and an optical analysis. In the finite element analysis, the mechanical deformation data of the secondary mirror surface is calculated, and then the optical analysis process is performed to predict the optical performance error using the deformation data. For the finite element analysis, CAD modeling of the structure of the focus mechanism and element, node, property and boundary conditions are applied to the model to calculate the deformation in the secondary mirror surface. The wavefront error of the optical surface is calculated by using the Zernike polynomial for the obtained deformation data of the optical surface.

In this research the finite element analysis was carried out by applying the focus mechanism with the flexure to the maximum tilt (x and y-axis Tilt: 200 μrad). From this, the deformation data of the secondary mirror surface were extracted. The deformation data of the secondary mirror surface was divided into Zernike polynomials and then wavefront errors of the secondary mirror surface

were obtained. In Zernike polynomials, deformation due to rigid body motion can be easily compensated through the mechanism, so the rigid body motion (de-space, tilts and de-center) terms are removed in the calculation of Zernike polynomials. The optical performance of the secondary mirror surface is determined by the RMS value of the wavefront error, which is composed of the remaining terms after eliminating rigid body motion. After conducting finite element analysis using ANSYS, Zernike polynomial dividing and wavefront error analysis were performed using MATLAB code.

The shape of the flexure was the same used in the previous study [6]. As a result, the RMS value of the wavefront error on the secondary mirror surface of the focus mechanism using the flexure is about 1.38 nm, which is about 24 times lower than that of the mechanism without the flexure. Table 2 shows the properties of the materials used in the finite element analysis. Fig. 4 is the wavefront error shape of the secondary mirror surface from which the rigid body motion terms are removed in the divided Zernike polynomial.

Table 2 Material Properties used for FEM Analysis

Material	Density [kg/m^3]	Young's Modulus [GPa]	Poisson's Ratio	Element (ANSYS)
Zerodur (Mirror)	2,530	91.3	0.24	SOLID95
EC-2216 (Adhesive)	1,140	0.565	0.47	SOLID95
Super Invar 32-5 (Flexure)	8,140	145	0.23	SOLID95

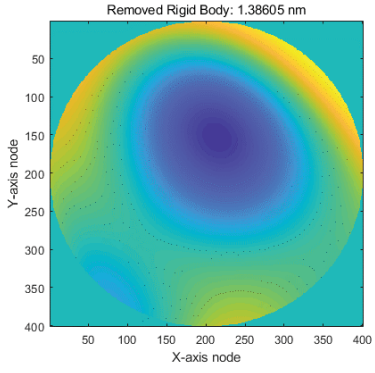

Fig. 4 Wave front Error of the Secondary Mirror

3. Servo Performance Verification of Focus Mechanism

3.1. Configuration of Focus Mechanism

A mock-up of the focus mechanism was designed and fabricated to evaluate the servo performance of the proposed focus mechanism. The secondary mirror for servo performance verification is made of aluminum with density similar to Zerodur. The Newport 8354 Picomotor was used as the PIFA, and the DP/0.5/S of Solartron was used as the displacement sensor. Mechanism controller design, operational test, and data acquisition were performed using LabView. The Picomotor 8354 has a stroke of 12.7 mm and a resolution of 20 nm per step. The DP/0.5/S has a measurable range of 0.5 mm and a resolution of 30 nm. Because of the characteristics of the Picomotor, bearings and support structures are used to exclude the rotational motion, as the rotor generates the linear displacement through rotation. Fig. 5 shows the focus mechanism configuration.

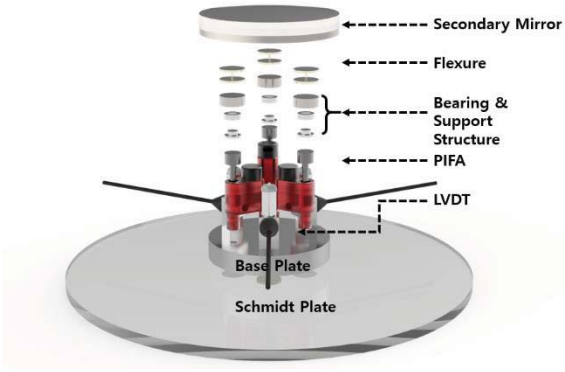

Fig. 5 Focus Mechanism Assembly using PIFAs and LVDTs

3.2. Modeling of PIFA

The PIFA used in this study is operated by rotating the rotor using the expansion-compression phenomenon in the longitudinal direction of the piezoelectric actuator. The working principle is as follows. The force applied from the piezoelectric actuator inside the PIFA is transferred to the flexure inside the motor, and then the flexure is deformed. The deformation of the flexure pushes out the engaged rotor and generates the linear displacement, and at that moment the piezoelectric actuator is rapidly compressed to maintain the linear displacement of the rotor. Fig. 6 shows the diagram of PIFA, which can be expressed as Equations (8) and (9).

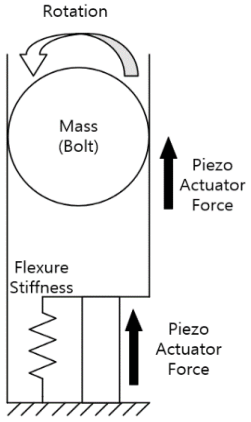

Fig. 6 PIFA Schematic Diagram

$$m_{piezo}\ddot{x} + c_{equiv}\dot{x} + k_{equiv}x = F_{piezo} \quad (8)$$

$$I_{bolt}\ddot{\theta} = (F_{piezo} - F_{fric})r \quad (9)$$

In equation (8), m_{piezo} is the mass of the piezoelectric actuator, c_{equiv} is equivalent to the damping constant of the actuator and flexure, k_{equiv} is equivalent stiffness of the piezoelectric actuator and flexure, and F_{piezo} is the force generated when the input voltage applies to the piezoelectric actuator. In equation (9), I_{bolt} is the moment of inertia of the rotor and F_{fric} is the friction force. The relationship between the input voltage and the piezoelectric actuator is as follows.

$$\alpha V(t) = \beta \frac{d}{dt} F_{Piezo} + F_{piezo} \quad (10)$$

In equation (10), α is a constant indicating the relationship of the equation, and β is the time constant of the piezoelectric actuator in PIFA. After taking the Laplace Transform of the above equations, it is the same as transfer function (input is voltage, output is displacement) given by Equation (11).

$$\frac{X(s)}{V(s)} = \frac{\alpha}{(\beta s + 1)(ms^2 + c_{equiv}s + k_{equiv})} \quad (11)$$

These constants can be estimated experimentally through an open loop experiment that drives the PIFA to produce the displacement. When the PIFA is driven, the voltage input per step is confirmed by oscilloscope. Fig. 7 (a) is the result of the oscilloscope measurement, and (b) is the graph of the input to the MATLAB.

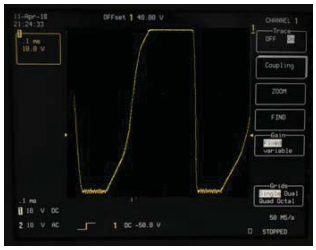

(a) Measured Voltage using Oscilloscope

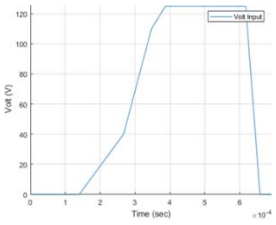

(b) MATLAB Input

Fig. 7 Input Voltage for PIFA

In the open loop experiment, the input voltage and the displacement of the PIFA were obtained. The transfer function of the PIFA was obtained by using the MATLAB system identification tool. The modeling of the PIFA is constructed in the form of the third order system as shown in Equation (11). The values of the constants are summarized in Table 3.

Table 3 Parameters of the PIFA

Coefficient	α	β	m_{piezo} [kg]	c_{equiv} [kg/s]	k_{equiv} [N/m]
Value	2,674	221.5 e-6	471 e-6	48,866	220.6 e6

3.3. Focus Mechanism Servo Performance Experiment

For the servo performance experiment of the focus mechanism using the PIFAs, we constructed the experimental interface with LabView as shown in Fig. 8, Fig. 9 shows the experimental equipment configuration. The closed loop is constructed by using LVDTs, and the servo performance of the system is improved by applying the PD controller. The experimental conditions were as follows: De-space: 10 μm, x, y Tilt: 200 μrad respectively. The PIFA was driven sequentially due to the power limitation of the driver. When the three PIFAs converge to the command within the error of 30 nm, the loop termination condition is set to terminate when satisfying the error condition.

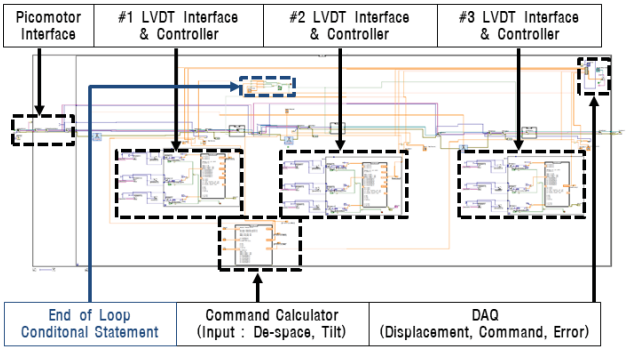

Fig. 8 Experimental Interface Configuration for the Focus Mechanism

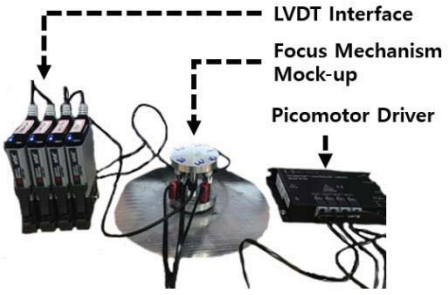

Fig. 9 Experimental Device Configuration for the Focus Mechanism

In the performance experiment, we designed the PD controller in Simulink of MATLAB using the modeling of the PIFA obtained in the previous section and then adjust the gains of the controller through an actual performance test. As a consideration in designing the controller, the D-controller is added to increase the damping ratio of the mechanism to improve overshoot and transient response. The gains of the controller obtained from the MATLAB simulation are (P-gain: 1.1, D-gain: 0.3). Next, the servo performance of the focus mechanism was improved through repeated experiments in the actual servo experiment, and the gains of the controller were determined to be (P-gain: 1.2, D-gain: 0.5). Simulink simulation results are shown in Fig. 10. Fig. 11 shows the servo performance test result of each PIFA for the specified de-space and tilt behavior. In the servo performance test, the steady-state error of each PIFA was confirmed to be within ± 0.03 μm, and the tilt error of the secondary mirror by the focus mechanism was confirmed to be within ± 0.8 μrad.

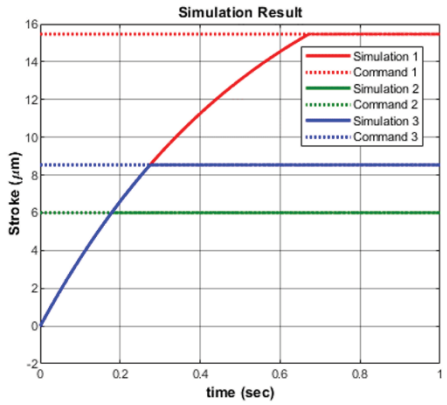

Fig. 10 Simulink Simulation Result

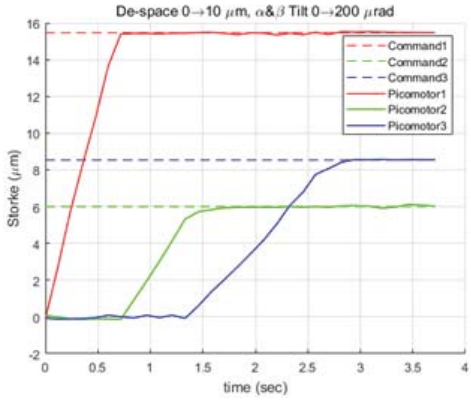

Fig. 11 Experimental Results of Focus Mechanism

4. Conclusions

In this study, we proposed a 3-axis focusing mechanism using PIFAs for the compensation of misalignment in a small satellite camera. This mechanism was applied to compensate for degradation in image quality due to misalignment occurring in the launch and space environments of small satellite cameras. The focus mechanism proposed in this study is applied to a satellite camera of 200 mm class Schmidt-Cassegrain type. Based on this, the size and the compensation range of the focus mechanism were set, and the design requirements were derived accordingly. The focus mechanism consists of three PIFAs to compensate for x, y-axis tilt and de-space, and the flexures between the PIFAs and the second mirror were installed to minimize optical performance degradation when the mechanism works. In order to calculate the wavefront error of the secondary mirror surface by the focus mechanism operation, the deformation data

was calculated through the finite element analysis and the wavefront error was calculated by substituting the deformation data of the surface into the Zernike polynomial. It was confirmed that the application of the flexure to the focus mechanism reduces the wavefront error of about 24 times compared to the case where the flexure is not applied under the maximum tilt condition. As a result of the position control experiment to verify the servo performance of the focus mechanism, the position accuracy of ± 0.03 μm was confirmed, which is less than the de-space requirement of 0.5 μm. In addition, the x and y-axis tilt error is ± 0.8 μrad which is below the tilt requirement of 5 μrad. Therefore, the results of this study confirm that the precise refocusing can be done by the 3-axis focus mechanism using a PIFA when misalignment occurs in small satellite cameras in launch and space environments. Through this study, basic valuable results for a 3-axis focus mechanism of a small satellite camera using PIFAs have been obtained.

Acknowledgement

This work was supported by Global Surveillance Research Center (GSRC) program funded by the Defense Acquisition Program Administration (DAPA) and Agency for Defense Development (ADD).

References

[1] G. S. Kim, "Development Trends in Super High-Resolution Earth Observation Optical Satellite," Current Industrial and Technological Trends in Aerospace, Vol. 11, No. 2, pp. 101-110, 2013.

[2] Y. S. Yoon and K. J. Min, "Industry Trend and Development Status of Nano/Micro Satellite," Current Industrial and Technological Trends in Aerospace, Vol. 14, No. 1, pp. 18-25, 2016.

[3] Y. Jang, M. Park, S. Yu, S. Park, and G. Choe, “The trend and prospect of small satellite formation flying technology,” *Journal of The Korean Society for Aeronautical & Space Sciences,* Vol. 31, No. 7, pp. 136-149, 2003.

[4] Braam Ben, H. A. van Mierlo, G. Buvril, S. Gill, “Meteosat Second Generation Refocusing Mechanism,” ESA – SP(European Space Agency - Special Publication), Vol. 410, pp. 27-34, 1997.

[5] J. S. Chang, J. U. Kim, M. S. Kang, S. U. Yang and E. E. Kim, "Development and Verification of Thermal Control Subsystem for High Resolution Electro-Optical Camera System, EOS-D Ver.1.0," *Journal of The Korean Society for Aeronautical and Space Sciences*, Vol. 41, No. 11, pp. 921~930, 2013.

[6] D. G. Hong and J. H. Hwang, “Design of 3-Axis Focus Mechanism Using Piezoelectric Actuators for a Small Satellite Camera,” *Journal of Aerospace System Engineering*, Vol. 12, No. 3, pp.9-17, 2018.

[7] D. H. Lee and J. H. Hwang, “An Online Tilt Estimation and Compensation Algorithm for a Small Satellite Camera,” Proceedings of The Asia-Pacific International Symposium on Aerospace Technology, pp. 1572-1582, 2017.

[8] R. D. Gehrz, E. A. Romana, W. F. Hoffmann, J. P. Schwenker, J. E. Mentzell, J. L. Hora, P. R. Eisenhardt, B. R. Brandl, L. Armus, K. R. Stapelfeldt, D. C. Hines, A. K. Mainzer, E. T. Young, and D. G. Elliott, “The state of the focus and image quality of the Spitzer Space Telescope as measured in orbit,” Proceedings of SPIE 5487, pp. 166-176, 2004.

[9] D. Kim, Y. Choi, M. Kang, E. Kim, and H. Yang, “Optical alignment of a high-resolution optical earth observation camera for small satellites,” *Korean Journal of Optics and Photonics* Vol. 15, No. 4, pp. 391-396, 2004.

[10] V.V. Klemas, Sensors and Techniques for Observing Coastal Ecosystems. In: Yang X. (eds) Remote Sensing and Geospatial Technologies for Coastal Ecosystem Assessment and Management. Lecture Notes in Geoinformation and Cartography. Springer, Berlin, Heidelberg, 2009.